JAERI-Research
2003-024

TRITIUM PERMEATION EVALUATION THROUGH VERTICAL TARGET OF DIVERTOR BASED ON RECENT TRITIUM TRANSPORT PROPERTIES

November 2003

Hirofumi NAKAMURA and Masataka NISHI

日本原子力研究所
Japan Atomic Energy Research Institute

本レポートは，日本原子力研究所が不定期に公刊している研究報告書です。
入手の問合わせは，日本原子力研究所研究情報部研究情報課（〒319-1195　茨城県那珂郡東海村）あて，お申し越しください。なお，このほかに財団法人原子力弘済会資料センター（〒319-1195　茨城県那珂郡東海村日本原子力研究所内）で複写による実費頒布をおこなっております。

This report is issued irregularly.
Inquiries about availability of the reports should be addressed to Research Information Division, Department of Intellectual Resources, Japan Atomic Energy Research Institute, Tokai-mura, Naka-gun, Ibaraki-ken, 319-1195, Japan.

編集兼発行　　日本原子力研究所

Tritium Permeation Evaluation through Vertical Target of Divertor based on Recent Tritium Transport Properties

Hirofumi NAKAMURA and Masataka NISHI

Department of Fusion Engineering Research
(Tokai site)
Naka Fusion Research Establishment
Japan Atomic Energy Research Institute
Tokai-mura, Naka-gun, Ibaraki-ken

(Received October 1, 2003)

Re-evaluation of tritium permeation through vertical target of divertor under the ITER operation condition was carried out using tritium transport properties in the candidate materials such as the diffusion coefficient and the trapping factors in tungsten for armor, and the surface recombination coefficient on copper for the heat sink obtained by authors' recent investigation (authors' data), which simulated the plasma-facing conditions of ITER. Evaluation with the data set of previous evaluation was also carried out for comparison (previous data). The permeation analysis was carried out individually by classifying into the armor region (Carbon Fiber Composites and tungsten) and the slit region without armor (3% of armor surface area) assuming the incident flux and temperature for each region. As the results of the permeation analysis, estimated permeation amount with the authors' data was one order less than that with the previous data at the end of lifetime of the divertor due to authors' small diffusion coefficient of tritium in tungsten. It also indicated the possibility that permeation through the slit region of the armor tiles could dominate total permeation through the vertical target, since tritium permeation amount through tungsten armor with the authors' data was estimated to be reduced drastically smaller than that with the previous evaluation data.

The result of a little tritium permeation amount through the vertical target with the authors' data ensured the conservatism of the current evaluation of tritium concentration in the primary cooling water in ITER divertor, as it indicated the possibility of direct drainage of the divertor primary cooling water.

Keywords; Tritium, Permeation, ITER, Divertor, Plasma Driven Permeation, Tungsten, CFC, Copper, Fusion Reactor

トリチウム輸送物性値の新知見に基づくダイバータ垂直ターゲットからのトリチウム透過評価

日本原子力研究所那珂研究所核融合工学部
中村　博文・西　正孝

(2003年10月1日受理)

ITERダイバータ部におけるトリチウムの冷却水への透過量の再評価を行った。本評価は、ITERの設計緒元を用い、著者らが近年の研究で得てきたタングステンや銅における水素同位体の輸送物性値(拡散係数、トラップ因子、表面再結合係数等)を用いて行ったものである。比較のためにこれまでの評価で用いられてきたタングステンや銅等の輸送物性値を用いた評価も同様に実施した。ダイバータは、アーマ材領域とアーマ材が存在しないスリット領域に分類し、それぞれの領域について評価した。解析の結果、著者らの新知見に基づくトリチウム透過の評価値は、従来の輸送物性値の報告値を使用した結果よりもダイバータ供用期間末期において1桁以上低い値となった。また、新知見によるトリチウム透過はダイバータタイルのスリット領域からの透過が支配的となる可能性を見出した。このような冷却水への少ないトリチウム透過量は、冷却水の直接排水の可能性をも示唆するように、現行のITERの運転期間中におけるダイバータ冷却水中トリチウム濃度の評価値が十分な安全裕度を有していることを確認するものである。

那珂研究所（東海駐在）：　〒319-1195　　茨城県那珂郡東海村白方白根2-4

Contents

目 次

1. Introduction

Tritium permeation through the fusion materials is one of critical issues in the DT fusion reactor such as ITER (International Thermonuclear Experimental Reactor) for the safety assessment or tritium inventory control etc, [1]. Especially, because it is expected the enhancement of tritium permeation called "plasma driven permeation" through the plasma facing components (PFC) exposed to the DT plasma, which means the exited state of DT particles such as ions or neutral atoms generated charge exchange reaction, it is desired to evaluate the tritium permeation amount through PFC to cooling water. In the design activity in ITER, tritium permeation and inventory analysis in the PFC has been carried out extensively using the transport properties such as diffusion coefficient, trapping factors (trap site density and trap energy), solubility, surface recombination coefficient, etc. [2]. Those evaluations have been carried out using the tritium transport properties extrapolated by classical diffusion model [3] with the protium or deuterium data, which predicts that the diffusion coefficient is proportional to the inverse of the square root of the mass, due to a few tritium transport properties data for the candidate materials of the ITER PFC, although there is uncertainty on reliability of the classical diffusion theory to estimate the isotope effect of the transport properties in materials [4]. Additionally, there still exist uncertainties on the transport properties in the plasma-facing surface under the high flux and low energy DT particles exposure expected in the vacuum vessel of the fusion reactor.

In such viewpoints, in order to analyze tritium permeation under the PFC conditions in the fusion devices, authors have been accumulated the tritium/deuterium transport properties such as diffusion coefficient, surface recombination coefficient, trapping factor and so on in the candidate materials of the PFC such as tungsten [5-7], copper [8] etc. [9,10] on the basis of the results of the ion driven permeation experiments using the experimental apparatus [11,12] which can produce low energy ($\leq$ 1 keV) and high flux pure tritium or deuterium ion beam ($\sim 1\times10^{19}$ ions/m^2s). Additionally, the evaluation method of tritium transport properties from the protium or deuterium data is also verified by comparing the transport properties between pure tritium and deuterium [13,14].

Based on those transport properties of the candidate materials, tritium permeation through divertor to the cooling system has been re-evaluated under the realistic operation scenario and divertor structure geometry of current design.

This paper reports the result of tritium permeation analysis focused on the effect of transport properties, and discusses the influence of the operation scenario on the permeation and main permeation pass through the vertical target of the divertor.

2. Analytical Method of Tritium Permeation Evaluation

TMAP code [15], which is a standard tritium simulation code in ITER, is used for this permeation analysis. In the analysis, tritium permeation behavior was simulated by solving the hydrogen isotopes transport and thermal response in the PFC under the ITER simulated conditions.

2.1. Tritium Transport in the Divertor Materials

Hydrogen isotopes transport in the materials I can be expressed by Eq. (1) and (2) using the mass balance in the material.

$$\frac{\partial C_i^I}{\partial t} + \nabla J_i^I = S_i^I - \frac{\partial C_i^{tI}}{\partial t}, \tag{1}$$

Here, C_i^I, J_i^I and S_i^I are concentration, diffusion flux, and source of hydrogen isotopes i in the material I, and C_i^{tI} is concentration of trapped hydrogen isotopes i in the material I.

$$J_i^I = -D_i^I\left(\nabla C_i^I + \frac{Q_i^{*I} C_i^I}{RT^2}\nabla T\right), \tag{2}$$

Here, D_i^I and Q_i^{*I} are diffusion coefficient and heat of transport of hydrogen isotopes i in the materials I, R and T are gas constant and absolute temperature. ∇C and ∇T are concentration gradient and temperature gradient, respectively.

As to the trapping effect shown in Eq. (1), the only one trap site in the material I was assumed in this evaluation. Therefore, it is expressed in Eq. (3) and (4),

$$\frac{\partial C_i^{tI}}{\partial t} = \frac{\alpha_{ti} C_t^{eI}}{N} C_i^I - \alpha_{ri} C_i^{tI}, \tag{3}$$

$$C_t^{eI} = C_t^{0I} - \sum_i C_i^{tI}, \tag{4}$$

here, C_i^{tI} is concentration of trapped hydrogen isotope i in the material I. C_t^{0I} and C_t^{eI} are concentration of the trap site and concentration of the vacancy trap site in the material I. N is concentration of lattice atom, α_{ti} and α_{ri} are trapping probability and de-trapping probability of hydrogen isotope i in the material I, respectively.

α_{ti}, α_{ri} can be expressed by Eq.(5) and (6), respectively.

$$\alpha_{ti} = \frac{D_i^I}{\lambda^{I2}}, \tag{5}$$

$$\alpha_{ri} = \nu_0 \exp\left(-\frac{E_t}{RT}\right), \tag{6}$$

Here, λ^I, ν_0 and E_t are jumping distance (lattice constant), vibration frequency ($\sim 10^{13}$) and trap energy of hydrogen isotope i in the material I, respectively.

2.2. Tritium Transport through Materials

As to the transport through the materials, the concentration of hydrogen isotope in the materials A and B can be expressed by Eq. (7) assuming the equilibrium between the materials A and B, since the

chemical potential of the hydrogen isotope in metal can be defined by the solution constant by the Sievert's law.

$$\frac{C_i^A}{K_S^A} = \frac{C_i^B}{K_S^B} \quad , \tag{7}$$

Here, K_s^I means Sievert's solution constant in the material *I*.

2.3. Tritium Transport across Surface of the Materials

Transport of hydrogen isotope across the material surface can be expressed by the following equations,

$$J_i = \sum_{m=1}^{k} a_{mi} J_m \quad , \tag{8}$$

$$J_m = K_{dm} P_m - \sum_{j,k} kr_{ij} C_j C_k \quad , \tag{9}$$

here, J_i and J_m are the flux of hydrogen isotope i from material to the surface and the flux of hydrogen isotopes molecule m from the materials to the surface. a_{mi}, K_{dm}, P_m, and kr_{jk}: are numbers of the hydrogen isotope atom i, dissociation factor of incident molecule from the gas phase to the material surface, partial pressure of hydrogen isotope molecule m, and recombination coefficient of molecule m composed of atom j and k. C_j and C_k are the surface concentration of atom j and k.

At the equilibrium between hydrogen - metal system, the surface concentration of hydrogen isotope on metal can be expressed by Sievert's law.

$$C_i = K_S P_m^{1/2} \quad , \tag{10}$$

2.4. Thermal Response of the Divertor Materials

The divertor surface will be exposed to the cyclic high heat load during the DT plasma operation. Since the tritium transport in the materials is strongly dependent on the material temperature, the thermal response of the divertor is evaluated using Eq. (11) for each divertor material.

$$\rho C_p \frac{\partial T}{\partial t} = \nabla(\kappa \nabla T) + S_h \quad , \tag{11}$$

Here, ρ, C_p, T, κ and S_h are material mass density, material specific heat, absolute temperature, thermal conductivity, and local volumetric heating rate in the material *I*.

By solving Eq. (11) under given boundary condition (see **3.5**), the thermal response can be evaluated. For the composite material, the gap conductance was considered as follows.

$$q = h_{gap}(T_{S2} - T_{S1}) \quad , \tag{12}$$

Here, q, h_{gap}, T_{S2} and T_{S1} are interface heat flux, gap thermal conductance, and surface temperature of *S2* and *S1* structure, respectively.

3. Analysis Model of Tritium Permeation through the Divertor

3.1. Structure of the Divertor

Outline of the ITER divertor is shown in Fig. 1 [16]. The surface of the vertical target of the divertor is covered with the armor materials such as tungsten or carbon fiber composite (CFC), and inside of the armor tiles consists of the heat sink of the copper alloy and the cooling tubes to transfer the heat to the coolant. In the current design of the divertor, the armor material structure has many slits to relieve the thermal expansion or heat deflection (Fig. 1 (b)). At the bottom of the slits, bare copper or brazing material faces to DT plasma, and the barrier for tritium permeation to the coolant is much less than armor area. Therefore, tritium permeation through the slit area due to the direct incidence of tritium into the bottom of the slit should be estimated, even if the area of the slit region is small and the tritium incident flux into the bottom will be quite smaller than the incident flux into the armor surface.

3.2. Classification of Tritium Permeation Analysis Region

Tritium permeation analysis was performed for three regions of the divertor of ITER; tungsten armor region, CFC armor region and copper heat sink at the slit region of the armor tiles. Figure 2 shows analytical geometry of three regions, (a) the tungsten armor region, (b) the CFC armor region and (c) heat sink (copper) region at the bottom of the slits, respectively, and the surface area of each region is assumed 145 m^2, 50 m^2 and 5 m^2, respectively. Here, the surface area of the slit is assumed about 3% of the tungsten armor area as a minimum estimation, since it depends on the detail design of the armor structure under development.

3.2.1. Analytical Geometry of the Tungsten Armor Region

The permeation pass in the tungsten armor region is shown in Fig. 2 (a). This system consists of the tungsten armor exposed to DT plasma and copper heat sink behind of the armor. In this analysis, thickness of tungsten armor and copper heat sink were assumed to be 10 mm and 4 mm, respectively.

For the hydrogen isotope transport in tungsten, it is known that the powder metallurgy tungsten, which is one of candidates of the ITER divertor armor, has strong trap effect and it decreases with the annealing at high temperature above 1273 K [17]. Authors have also revealed this phenomenon with the permeation experiment of tritium or deuterium implanted into several tungsten specimens. It is that tritium/deuterium transport in annealed tungsten could be expressed with an effective diffusion coefficient, which involves the weak trapping parameter, and that it could be expressed with the combination of the effective diffusion coefficient and trap effect in the un-annealed tungsten [6]. Additionally, authors have

revealed that the diffusion coefficient in the implantation region of the tungsten was larger than that in the bulk tungsten by several times [13]. Since the surface temperature of the armor region is expected to be higher than 1273 K by the heat load of the DT plasma, tungsten armor of 10 mm thick was classified into three regions that are implantation zone within 10 nm depth (W-A), annealed zone within 3 mm depth (W-B) and un-annealed zone from 4 mm to 10 mm depth (W-C). Copper heat sink region was assumed to be a single region of 4 mm thick (W-D) as shown in Fig. 2 (a).

3.2.2. Analytical Geometry of the CFC Armor Region

For the CFC armor region, cooling tubes are located inside of the CFC block of 30 mm thick as shown in Fig. 2 (b). Main permeation pass in the CFC armor region can be the migration in near surface region of the CFC block and the copper cooling tube after the implantation of low energy DT plasma into the CFC armor. In this analysis, it is assumed that the analytical geometry of the CFC consists of the CFC armor of 10 mm thick and copper cooling tube of 4 mm thick to simulate the shortest tritium permeation pass.

In this CFC armor region, the CFC layer is classified into 2 regions that are 10 nm implantation zone (CFC-A) and 10 mm CFC block (CFC-B), and copper area is assumed to be a single region of 4mm thick (CFC-C).

3.2.3. Analytical Geometry of the Heat Sink Region

For the analysis of copper heat sink at the bottom of the slit of armor tiles, permeation pass can be the diffusion in copper heat sink exposed to the atomized DT flux at the bottom of the slits of the armor tiles. The copper block is classified into 2 regions that are 10 nm implantation zone (Cu-A) and ~4 mm copper block (Cu-B) as shown in Fig. 2 (c).

3.3. Tritium Transport Properties of Materials and Boundary Conditions for the Permeation Analysis

Table 1 summarizes the tritium transport properties and thermal properties of the tungsten, CFC and copper used in this evaluation. Here, tritium permeation evaluation is carried out using the two methods; one is the evaluation with the properties reported by the authors, which are obtained with the ion driven permeation experiments of tritium and deuterium using low energy high flux ion beam (authors' data) [6-8,18], and the other is evaluation with the properties used in previous evaluation (previous data) [2, 17,19-26] for comparison.

For the tritium transport properties of authors' data of tungsten, diffusion coefficient in the implantation region and the bulk, and trapping factor obtained with the permeation experiment with 1keV tritium or deuterium ion implantation [7,8,13] were used. Here, the authors' tritium diffusion coefficient is only data obtained with tritium in tungsten. The trapping factor of tritium in tungsten is assumed to be

same with deuterium.

For the tritium transport properties of authors' data of copper, the surface recombination coefficient of tritium on the copper surface was extrapolated by the deuterium data obtained by the permeation experiment with 200 eV deuterium ion implantation in a following method. The surface recombination coefficient can be expressed in Eq. (13) with the solubility (*Ks*, $Ks=Ks_0 exp(-Es/RT)$) by the Pick model [27],

$$kr = \frac{\alpha\phi_i}{Ks_0^{\,2}} \exp\left(-\frac{2E_S - 2E_c}{RT}\right), \tag{13}$$

here, α: implantation probability, ϕ_i: implantation flux, *Ec*: surface potential barrier, *R*: gas constant, and *T*: absolute temperature.

According to the isotope effect of solubility of hydrogen in fcc metal proposed by Ebisiuzaki [28], ratio of the solubility between isotopes α and β can be expressed in Eq. (14),

$$\frac{Ks^{\alpha}}{Ks^{\beta}} = \left(\frac{m^{\beta}}{m^{\alpha}}\right)^{-3/2} \left(\frac{g\left(\theta^{\beta}/\sqrt{m^{\beta}T}\right)}{g\left(\theta^{\alpha}/\sqrt{m^{\alpha}T}\right)}\right)^{3} \exp\left(\frac{\Delta G_0^{\alpha} - \Delta G_0^{\beta}}{2RT}\right), \tag{14}$$

here, *m*: mass number, *ΔG*: difference of the free energy of solution.

$g(x) \equiv (2/x)\sinh(x/2)$, θ: characteristic vibration temperature, ($\theta = h\nu/k$), *h*: Planck constant, *k*: Boltzmann constant, *v*: vibration frequency at ground state.

The ratio of the surface recombination coefficient between isotopes α and β can be expressed in Eq. (15) with Eq. (13) and (14).

$$\frac{kr_{\alpha}}{kr_{\beta}} = \left(\frac{m^{\beta}}{m^{\alpha}}\right)^{3} \left(\frac{g\left(\theta^{\beta}/\sqrt{m^{\beta}T}\right)}{g\left(\theta^{\alpha}/\sqrt{m^{\alpha}T}\right)}\right)^{-6} \exp\left(-\frac{\Delta G_0^{\alpha} - \Delta G_0^{\beta}}{RT}\right), \tag{15}$$

Since the authors revealed that the surface recombination coefficient of deuterium on copper surface exposed to deuterium ion implantation (<1 keV) could be expressed by the Pick model assuming *Ec*=0 (clean surface) [8] and that the isotope effect of the surface recombination coefficient between tritium and deuterium can be expressed by the Ebisuzaki's model (Eq. (15)) for fcc metal (for nickel) [14], the surface recombination coefficient of tritium can be evaluated using Eq. (15).

On the other hand, diffusion coefficient in the implantation region under the deuterium ion implantation (<1 keV) can be evaluated to be 10 times larger than that in the bulk of copper [8], which is available by using Katz's data [22].

For the properties of the CFC, there are still uncertainties on the tritium transport in CFC. Therefore, two previous data sets are used for the analysis; one is the combination of large diffusion coefficient and strong trap effect (case1) [20], and the other is small diffusion coefficient and weak trap effect [21]. Finally, the heat of transport (Q^* in Eq. (2)) is assumed to be zero for all materials in this analysis, because the effect of thermal diffusion (tritium diffusion induced by the thermal gradient) could be negligible. Figure 3 shows the transport properties such as (a) diffusion coefficient, (b) trapping factor

(trap site density and trap energy) and (c) recombination coefficient for tungsten, CFC and copper of authors' data and previous data. Here, the "common" in Fig. 3 (c) means common data between authors' data and previous data.

The boundary conditions for the tungsten armor surface faced DT plasma is assumed to be expressed in Eq. (8) and (9) except for the case with the authors' data (surface concentration is assumed to be zero), because experimental result by the authors' indicated that the tritium transport in the implantation region of tungsten is controlled by the diffusion process [6-8], and this assumption is also supported by the steady state hydrogen transport model proposed by Doyle and Brice [24]. Saturation model at the implantation region during the high flux DT plasma exposure proposed by Longhurst et al. [29] is not assumed in this analysis in order to verify the influence of the transport properties accurately. On the other hand, equilibrium of hydrogen isotope migration at the interface between the cooling tube and cooling water is assumed as expressed in Eq. (10). Here, the partial pressure of hydrogen isotope (D and T) in the cooling water is assumed to be zero.

3.4. Operational Scenario

In this analysis, two operation scenarios: a scenario of the short DT discharge period (scenario A) and a scenario of the long DT discharge period (scenario B), are assumed. In the scenario A, which is expected in the early phase of ITER operation, it is assumed the 16 discharges of 400 s of DT plasma (1400 s duration period) for a day (8 hrs operation/day). On the other hand, in the scenario B, which is expected in the engineering phase of ITER operation, it is assumed 44 discharges of 3000 s of DT plasma (9000 s duration period) for a week (24 hrs operation/day). Baking of the vacuum vessel (513 K for 6 hrs) is also assumed daily for the scenario A and weekly for the scenario B. The operation is assumed the 9 cycles per year, and 1 cycle is assumed the 2 weeks operation per 3 weeks. Tritium permeation evaluation was carried out for the scenario A and B for both without baking (A1and B1) and with baking (A2 and B2). Table 2 summarizes the operation conditions of assumed scenarios.

3.5. Heat Load and Particle Load of the Divertor

Surface temperature of the armor of the divertor will increase above 1273 K when it is exposed to the DT plasma, since the heat load of divertor surface is estimated to be 0.25~5 MW/m^2 during the DT discharge [2]. In this analysis, thermal response of the armor surface is evaluated under the conditions of the armor surface temperature of 1273 K during the discharge period and 423 K at duration period, and the cooling water temperature of 423 K. On the other hand, the thermal response of the copper heat sink is evaluated under the conditions of the surface temperature of the heat sink of 513 K during the discharge and 423 K at duration period, and the cooling water temperature of 423 K. Temperature distribution in the divertor materials is evaluated using Eq. (11) and (12) under the above surface temperature conditions.

For the particle load of the divertor, 3×10^{23} D, T/m^2s (D/T=1) of the incident flux is assumed for

the armor region (tungsten and CFC) as a most serious particle load of the divertor. On the other hand, the particle load of the bottom of the slits region is estimated to be attributed to the charge exchange particle from the DT plasma. Though it is difficult to evaluate accurately to estimate the particle load of the charge exchange particle to the bottom of the slits, 3×10^{17} ~3×10^{21} D, T/m^{2}s (D/T=1) of the particle loads [30] are assumed, which corresponds to 10^{-6} ~ 0.01 of the armor region. The implantation depth of the DT particle into the divertor is assumed to be 2.5 nm for tungsten armor and for copper heat sink region and 5 nm for the CFC region on basis of the TRIM calculation [31] of the range of hundreds eV of D and T. Figure 4 shows the boundary conditions of the surface temperature of the divertor and particle load of the surface for the scenario A and B, and Table 3 summarizes the set value of the surface temperature, the incident flux into the surface, the implantation range and effective area of each analytical region.

4. Results and Discussions

4.1. Tritium Permeation through Individual Analytical Region

Figure 5 (a) and (b) show the results of tritium permeation analysis through the tungsten armor region (scenario B2) and the copper heat sink region (scenario B2, 0.1% of the incident flux into the armor surface), respectively. For the CFC armor region, significant tritium permeation for both case 1 and 2 was not evaluated during the expected minimum lifetime of the divertor (27 cycles) under the operation scenario summarized in Fig.4 and Table 2 and 3. Here, Fig. 5 shows the comparison of time evolution of tritium permeation rate and permeation amount per unit area between authors' data and previous data. Figure 6 shows the total tritium permeation amount and permeation amount through each region after 27 cycles (~3years) operations under the various operation scenarios using the authors' data and those using previous data under the scenario B2 for comparison. Here, permeation amount through the copper heat sink is evaluated under the incident flux of 3×10^{20} D, T/m^{2}s (0.1% of flux into the armor surface). Significant tritium permeation through the tungsten armor and the copper region and negligible tritium permeation through the CFC armor region are expected as shown in Fig. 6. It can be also seen in Fig. 6 that the significant dependence of tritium permeation amount on the operation scenario or transport properties. As to the operation scenario dependency, the results indicate the scenario B, which means longer particle load and longer high temperature of the surface, enhances tritium permeation by several times at the copper region and several orders at the tungsten region, respectively. On the other hand, tritium permeation amount will increase by about several tens % by the baking at 513 K for 6 hrs.

4.2. Effect of Transport Properties on Tritium Permeation

As shown in Fig. 6, total tritium permeation amount evaluated by previous data is greater than that by the authors' data by several times. The main permeation pass for the previous data case is the armor region as seen in Fig. 6, it is mainly attributed to the break through of tritium permeation after 20 cycles just before the lifetime of the divertor (27 cycle) as shown in Fig. 5 (a). Since diffusion coefficient

of literature's data is quite larger than that of authors' data as shown in Fig. 3 (a), the permeation rate increases drastically once the trap sites has occupied in the tungsten region, although strong trap effect is assumed in tungsten region for the previous data case (Fig. 3 (b)). On the other hand, the main permeation pass for the authors' data is the copper heat sink region due to the quite small tritium permeation amount through tungsten armor region as shown in Fig. 6.

Assuming that total water hold up of the primary cooling water of divertor region is 145 m^3 [32], the tritium concentration in the primary water after the 3 years operation under the scenario B2 is expected to increase 26 GBq/m^3 by previous data and 1 GBq/m^3 by the authors' data, respectively. The results indicate that evaluation values with both authors' data and previous data can satisfy the concentration criteria of operation of the water detritiation system (37 GBq/m^3) [33]. If permeation through the copper region can be protected, tritium concentration in the cooling water can be reduced to about 10 MBq/m^3 which is near to the criteria of the environmental release concentration of tritiated water (6 MBq/m^3) for the scenario B2, since the tritium permeation amount evaluated with authors' data is dominated by the permeation through copper region under the incident flux of 0.1% of the incident flux of armor region.

4.3. Tritium Permeation Pass through the Vertical Target of the Divertor

For the evaluation with authors' data, it is indicated that the copper heat sink is a main permeation pass in the divertor for 0.1% of the incident flux of the armor surface (3×10^{20} D, T/m^2s). Since the incident flux into the bottom of the slits is difficult to evaluate as mentioned previously, evaluation of tritium permeation under the various incident flux into the copper heat sink has been carried out. Figure 7 shows results of permeation amount through the copper region when the incident flux into the copper is varied from 3×10^{17} to 3×10^{21} D, T/m^2s (D/T=1) (It is corresponds to 10^{-6} to 0.01 of incident flux of the armor surface). Although the permeation amount through the copper region decreases with the incident flux decrease, the copper heat sink is still major permeation pass even at the 10^{-5} of the incident flux into the armor surface as shown in Fig. 7. Since the permeation evaluation with the literature's data derives the larger tritium permeation amount through the tungsten armor region, the permeation through the copper area can be neglected. However, results of present evaluation with new transport properties by the authors, which derives quite a little permeation through the tungsten region, indicates possibility of significant tritium permeation through the copper region at slits of the armor tiles by bypassing the armor layer. Certainly, it depends on the incident flux into the bottom of the slit. It cannot be excluded without consideration on it, because there exists the possibility of the reflection of atomic hydrogen isotopes on the metal surface [34]. Therefore, the further knowledge on the incidence of the atomized or ionized tritium into the bottom of slits or the consideration of the permeation protection method is required in order to evaluate the accurate tritium permeation amount through the PFC.

5. Summary

Tritium permeation evaluation through the vertical target of the divertor was carried out with the tritium transport properties such as diffusion coefficient, and the trapping factors in tungsten for the armor, and the surface recombination coefficient on copper for the heat sink based on the ion driven permeation experiment using low energy and high flux pure tritium and deuterium ion beam performed by authors. Evaluation with the data set of previous evaluation performed in the activity of ITER EDA was also carried out for comparison.

The analysis was carried out individually by classifying into the armor region and the slit region without armor (3% of armor surface area) assuming the incident flux and temperature for each region.

As the results, it was found that total tritium permeation amount through the divertor with authors' data was about one order less than that with previous data at the end of lifetime of the divertor due to our small diffusion coefficient of tritium in tungsten. For the permeation through individual region, it was found that tritium permeation through CFC armor region could be negligible, and tritium permeation through the tungsten armor and the slits region could be estimated significant for both cases. The results also indicated possibility that permeation through the slit region of the divertor tiles could dominate the total permeation through the vertical target of the divertor for the authors' case, since the evaluation result of tritium permeation amount through tungsten armor with authors' data reduced drastically than that with the previous evaluation data.

The result of only a little tritium permeation amount through the divertor with authors' data ensured the conservatism of the current evaluation of tritium concentration in the primary cooling water in ITER divertor, as it indicated the possibility of direct drainage of the divertor primary cooling water.

Acknowledgements

The authors would like to thank Drs. S. Seki, H. Takatsu, H. Tsuji of Department of Fusion Engineering and Research. The authors also would like to thank Dr. T. Hayashi of Tritium Engineering laboratory for his helpful discussion and Drs. Y. Neyatani and S. O'hira of Safety Design Division of Department of ITER project for their information on the ITER operation scenario. Finally, the authors would like to thank Dr. M. Enoeda for his comments on this report.

References

[1] I. Takagi and K. Yamaguchi, Journal of Plasma and Fusion Research, **73** 1319 (1997). (in Japanese).

[2] G. Federicci, R. Anderl, J. N. Brooks, R. Causey, J. P. Coad, et al., Fusion Eng. Des. **39-40** 445 (1998).

[3] C. Wert and C. Zener, Phys. Rev. **76** 1167 (1949).

[4] J. Völkl and G. Alefeld, in "Diffusion in solid" eds. A. S. Nowick & J. J. Burton, Academic Press, New York (1975).

[5] H. Nakamura, T. Hayashi, M. Nishi, M. Arita and K. Okuno, Fusion Eng. Des. **55**, 513 (2001).

[6] H. Nakamura, T. Hayashi, Y. Iwai and M. Nishi, Fusion Technology, **39** 894 (2001).

[7] H. Nakamura, T. Hayashi, T. Kakuta, T. Suzuki and M. Nishi, J. Nucl. Mater. **297** 285 (2001).

[8] H. Nakamura, W. Shu, T. Hayashi, S.O'hira M. Nishi and M. Sugisaki, Fusion Science and Technology, **41** 887 (2002).

[9] H. Nakamura, T. Hayashi, S, O'hira, M. Nishi, and K. Okuno, J. Nucl. Mater. **258-263**, 1050 (1998).

[10] H. Nakamura, T. Hayashi, S. O'hira and M. Nishi, JAERI-Research 2001-042 (2001).

[11] K. Okuno, S.O'hira, H.Yoshida, Y. Naruse, et al., Fusion Technology **14** 713 (1988).

[12] H. Nakamura, Study of tritium permeation through plasma facing materials in fusion reactor, doctoral thesis (2002) (In Japanese).

[13] H. Nakamura, W. Shu, T. Hayashi and M. Nishi, J. Nucl. Mater. **313-316** 675 (2003).

[14] H. Nakamura, M. Nishi and M. Sugisaki, JAERI-Research 2003-018 (2003).

[15] G. R. Longhurst, D. F. Holland, J. L. Jones and B. L. Merrill, EGG-FSP-10315 (1998).

[16] G. Janeschitz, T. Ando, A. Antipenkov, V. Barabash, S. Chiocchio et al., Fusion Eng. Des., **39-40** 178 (1998).

[17] R. A. Anderl, D. F. Holland, G. R. Longhurst, et al., Fusion Technol. **21** 745 (1992).

[18] H. Nakamura, S. O'hira, M. Nishi, T. Venhaus, R. Causey et al., Proc. of 18th IEEE/NPSS Symposium of Fusion Engineering (SOFE99), 271-274 (2000).

[19] R. Frauenfelder, J. Vac. Sci. Technol. **6** 388 (1969).

[20] K. L. Wilson, FED-INTOR Report phase-2A 272 (1982).

[21] K. Morita, K. Ohtsuka and M. Hasebe, J. Nucl. Mater., **162-164** 990 (1989).

[22] L.Katz,M. Guinan and R. J. Borg, Phys. Rev. **B4** 330 (1971).

[23] E. Fromm and E, Gebhardt, "Gase und Kohlenstoff in Metallen", Springer-Verlag, 1976.

[24] B. L. Doyle and B. K. Brice, Raddiation Effects, **89** 21 (1985).

[25] I. Smid, M. Akiba, G. Vieder, L. Pochl,, J. Nucl. Mater., **258-263** 160 (1998).

[26] V. Barabash, M. Akiba, J.P. Bonal, G. Federrici, R. Matera et al., J. Nucl. Mater., **258-263** 149 (1998).

[27] M. A. Pick and K. Sonnenberg, J. Nucl. Mater. **131** 208 (1985).

[28] Y. Ebisuzaki, W. J. Kass, and M. O'Keeffe, J. Chem. Phys., **46** 1373 (1967).

[29] G. Longhurst, R. A. Anderl, R. A. Causey, G. Federici, A. A. Haasz, R. J. Pawelko, J. Nucl. Mater., **258-263** 640 (1998).

[30] ITER Plant Description Documents, 2.3 Divertor, (International Thermonuclear Experimental Reactor, (2002)).

[31] J. F. Ziegler, "The Stopping and Range of Ions in Matter", Pergamon Press, 1985.

[32] ITER Plant Description Documents, 3.3 Cooling Water, (International Thermonuclear Experimental Reactor, (2002)) .

[33] Y. Iwai, private communication.

[34] I. Takagi, K. Toyoda, M. Katayama, H. Fujita, K. Higashi, J. Nucl. Mater., **258-263** 1082 (1998).

Table 1 Tritium transport properties (A) and thermal properties (B) of the divertor materials

		W		CFC		Cu	
		Authors' data	Data used in previous evaluation	Case 1	Case 2	Authors' data	Data used in previous evaluation
A	D_b	D_0:6.74×10^{-8} m^2/s E_D: 0.73 eV [7]	D_0: 4.1×10^{-7} m^2/s E_D: 0.37 eV [19]	D_0:7.0×10^{-7} m^2/s E_D: 0.5 eV [20]	D_0:1.0×10^{-17} m^2/s E_D: 0.2 eV [21]	D_0: 6.2×10^{-7} m^2/s E_D: 0.378 eV [22]	
	D_f	D_0: 6.74×10^{-7} m^2/s E_D: 0.73 eV [13]	D_0: 4.1×10^{-6} m^2/s E_D: 0.37 eV	D_0: 7.0×10^{-6} m^2/s E_D: 0.5 eV	D_0: 1.0×10^{-16} m^2/s E_D: 0.2 eV	D_0: 6.2×10^{-6} m^2/s E_D: 0.378 eV [8]	
	Ks	Ks_0:1.87×10^{24} atom/m^3-Pa$^{0.5}$ E_S: 1.04 eV [17]		Ks_0:9.0×10^{21} atom/m^3-Pa$^{0.5}$ E_S: 1.45 eV [13]		Ks_0:4.1×10^{23} atom/m^3-Pa$^{0.5}$ E_S: 0.37 eV [23]	
	C_t^0	40ppm (W-C) [6]	29ppm (W-B) [17] 69ppm (W-C) [17]	10% [20]	10ppm [21]	kr_0: 1.27×10^{-23} m^4/s E_{kr}: -0.5 eV [8]	kr_0: 1.3×10^{-24} m^4/s E_{kr}: 0.03 eV [24]
	E_t	0.9eV (W-C) [6,18]	1.42eV (W-B) [17] 1.54eV (W-C) [17]	2.35 eV [20]	0.25 eV [21]	-	
	kr	-	kr_0: 7.1×10^{-18} m^4/s E_{kr}: 0.81 eV [17]	kr_0: 3.8×10^{-28} m^4/s E_{kr}: 0.45 eV [20]		-	
B	κ	163.0-0.0739T W/mK [25]		550.0-0.648 T+3.2E-4T^2 W/mK [26]		420.0-0.0643T W/mK [26]	
	C_p	0.14 J/gK (at RT) [25]		1.84 J/gK (at RT) [26]		0.39 J/gK (at RT) [26]	

Here, D_b: bulk diffusion coefficient, D_f: diffusion coefficient in the implantation region, Ks: Sievert's constant, C_T^0: trap site density, E_t:trap energy, kr: recombination coefficient, κ:thermal conductivity, C_p: specific heat

Table 2 Operational condition of the scenario A and B

Scenario	DT discharge time	Interval time	Shot /day	Operation hrs/day	Operation days /week	cycle	cycle/year	Baking(**D**)
A1	400 s	1400 s	16	~8 hrs	5 days	2weeks operation/3weeks	9	No
A2								513 K, 6 hrs daily
B1	3000 s	9000 s	~7	24 hrs	6 days			No
B2								513 K, 6 hrs weekly

Table 3 Set value of the particle load, implantation depth and thermal condition of the divertor surface during the DT discharge.

Region	ϕ_0 (D,T/m^{2}s (D/T=1))	Rp (nm)	T_0(K)	Area (m^2)
Tungsten armor	3.0×10^{23}	2.5	1273 K	145
CFC armor	3.0×10^{23}	5	1273 K	50
Copper heat sink	3.0×10^{18} ~3.0×10^{22}	2.5	513 K	5 (slit region)

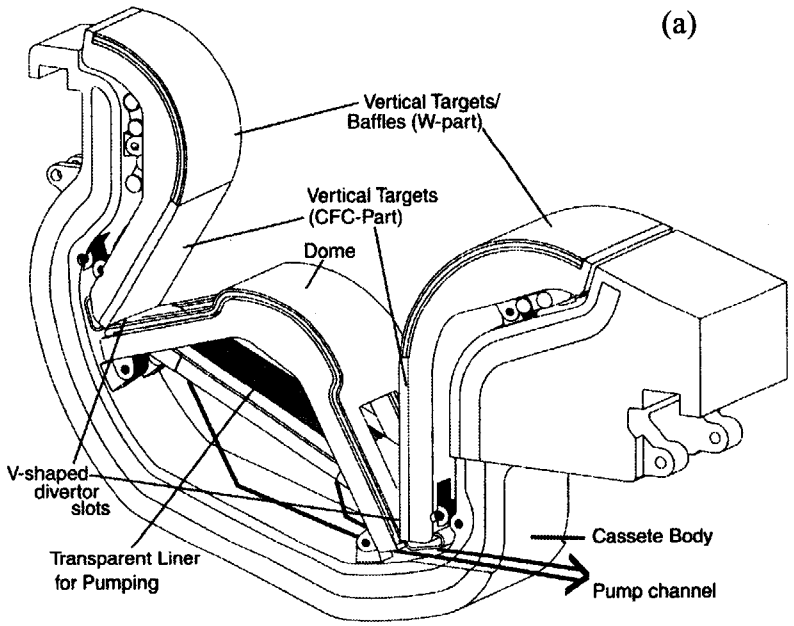

Fig. 1 Divertor structure
(a) Outline of the divertor cassette,

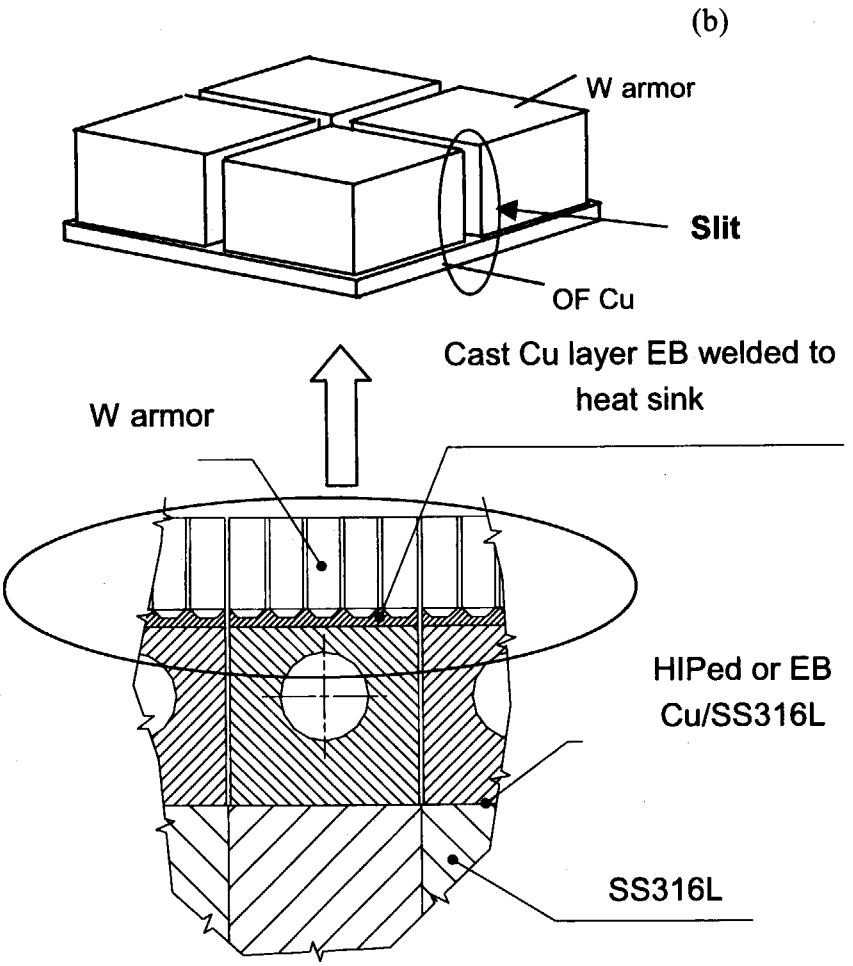

Fig. 1 Divertor structure
(b) Cross sectional view of tungsten armor of the divertor

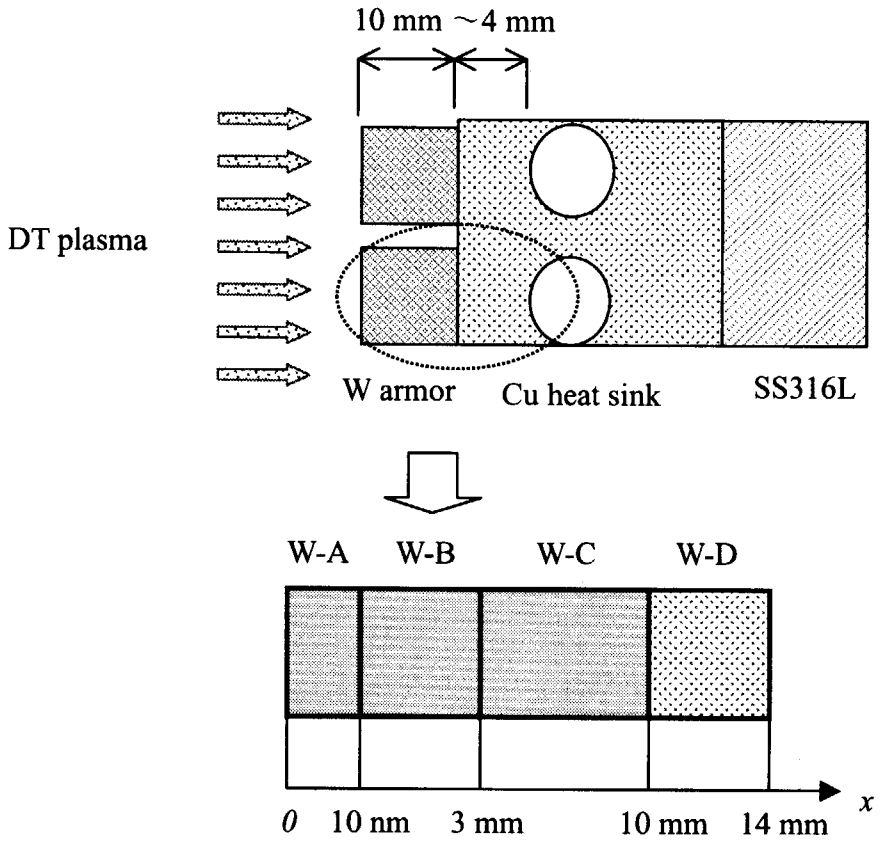

Fig. 2 Analytical geometry for the TMAP calculation of tritium permeation analysis.
(a) Tungsten armor region,

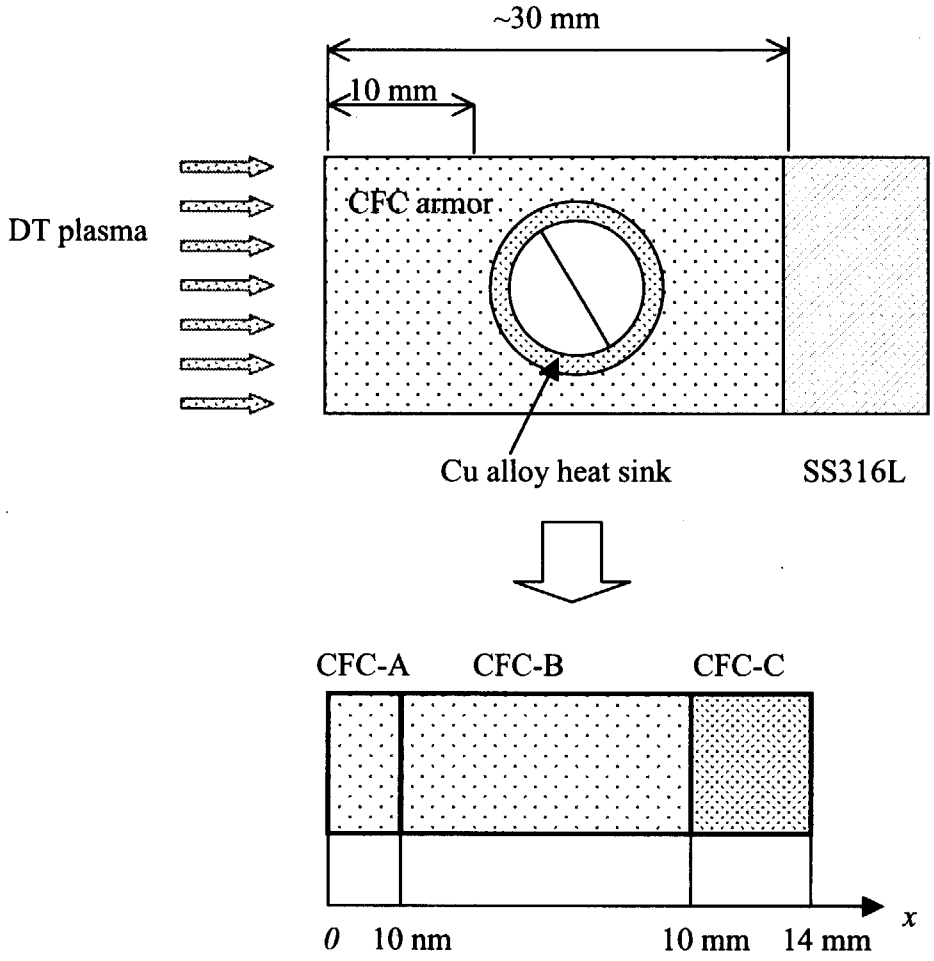

Fig. 2 Analytical geometry for the TMAP calculation of tritium permeation analysis.
(b) CFC armor region

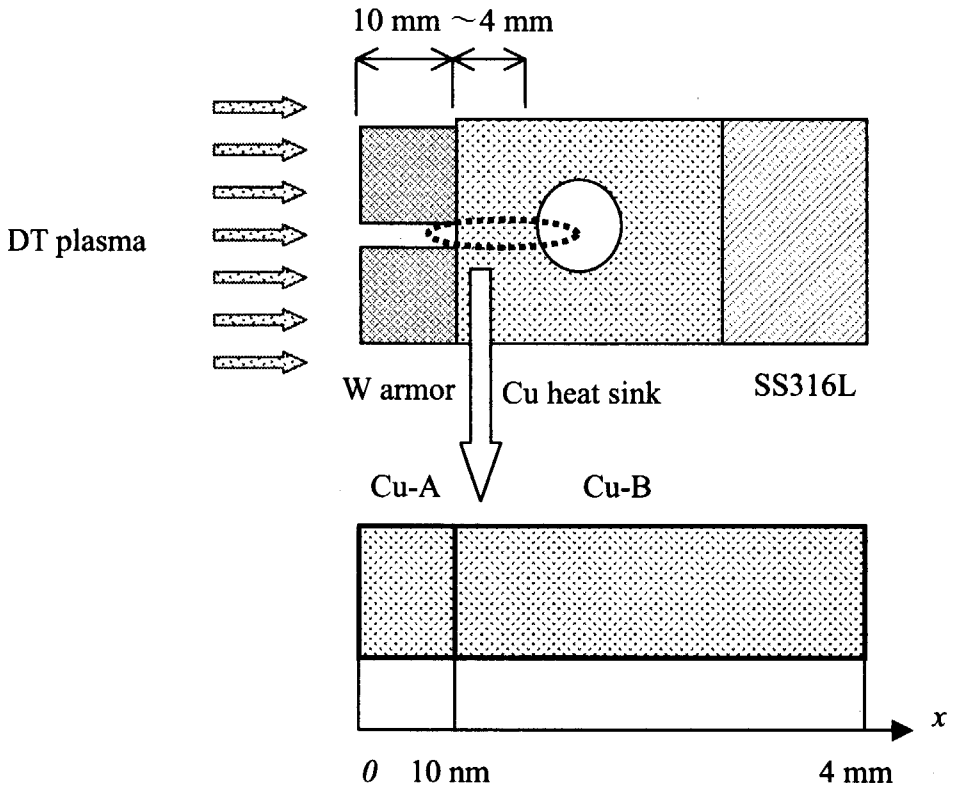

Fig. 2 Analytical geometry for the TMAP calculation of tritium permeation analysis.
(c) Copper heat sink region

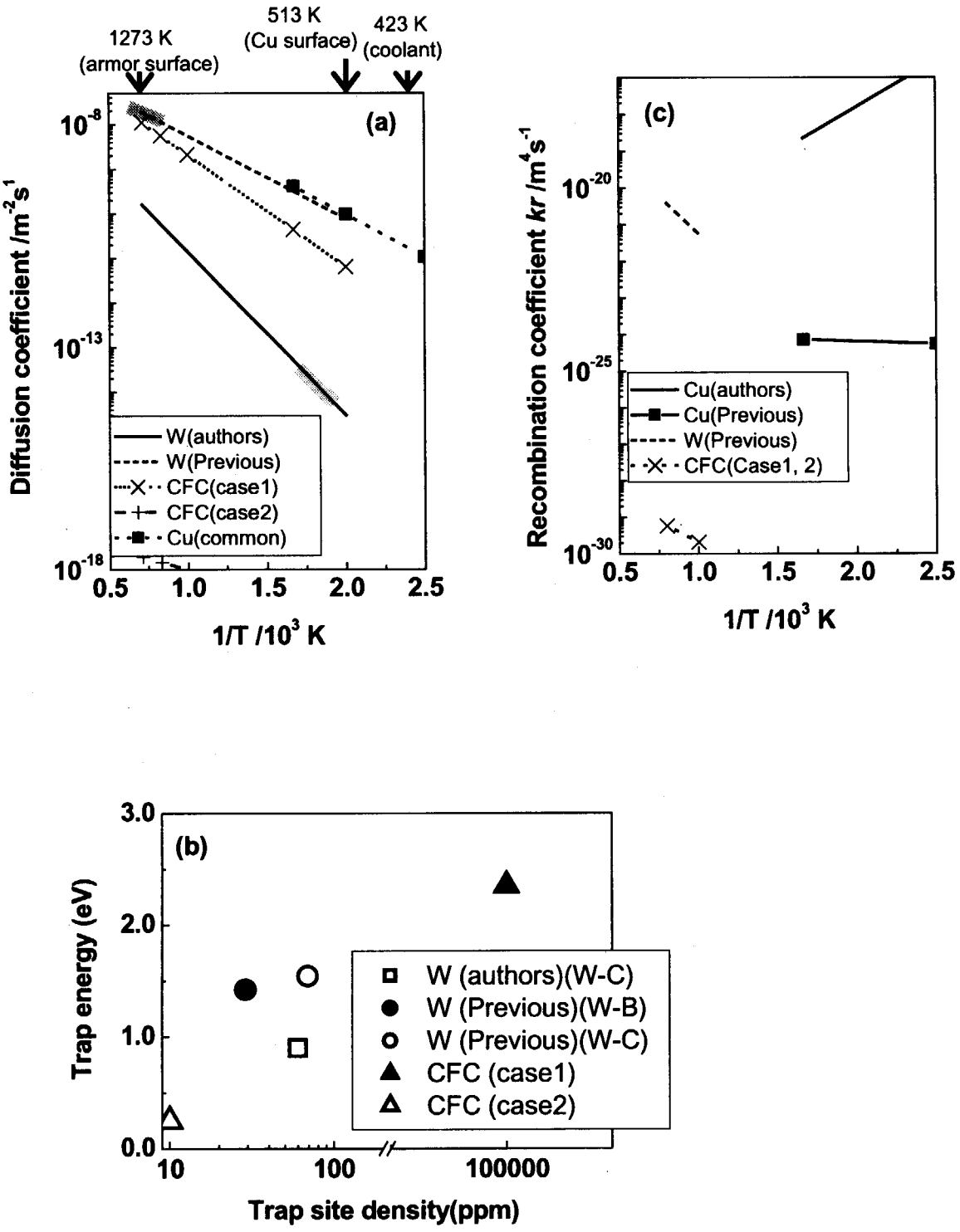

Fig. 3 Tritium transport properties in the divertor materials.

(a) Diffusion coefficient, (b) Trap site density and trap energy, and (c) Recombination coefficient. Here, bold lines mean experimental temperature ranges of reported properties.

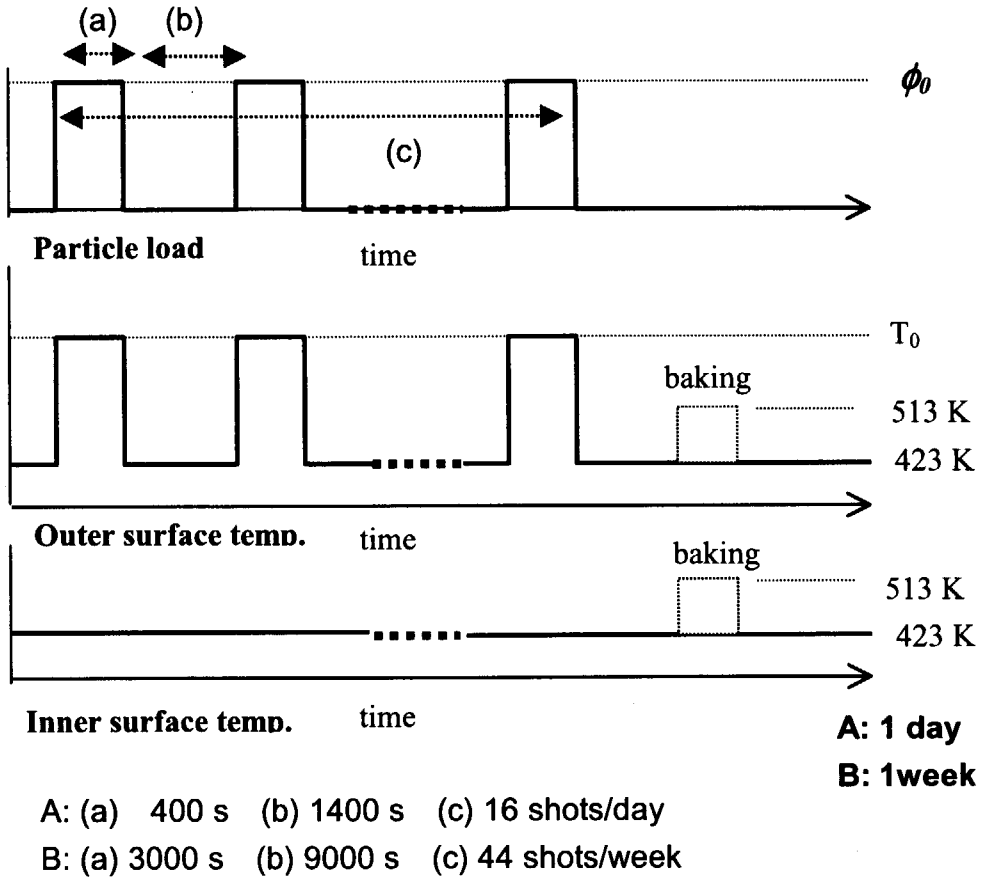

Fig. 4 Scenario of the heat load (temperature set value) and particle load into the divertor surface. Here A and B mean scenario A and B, respectively

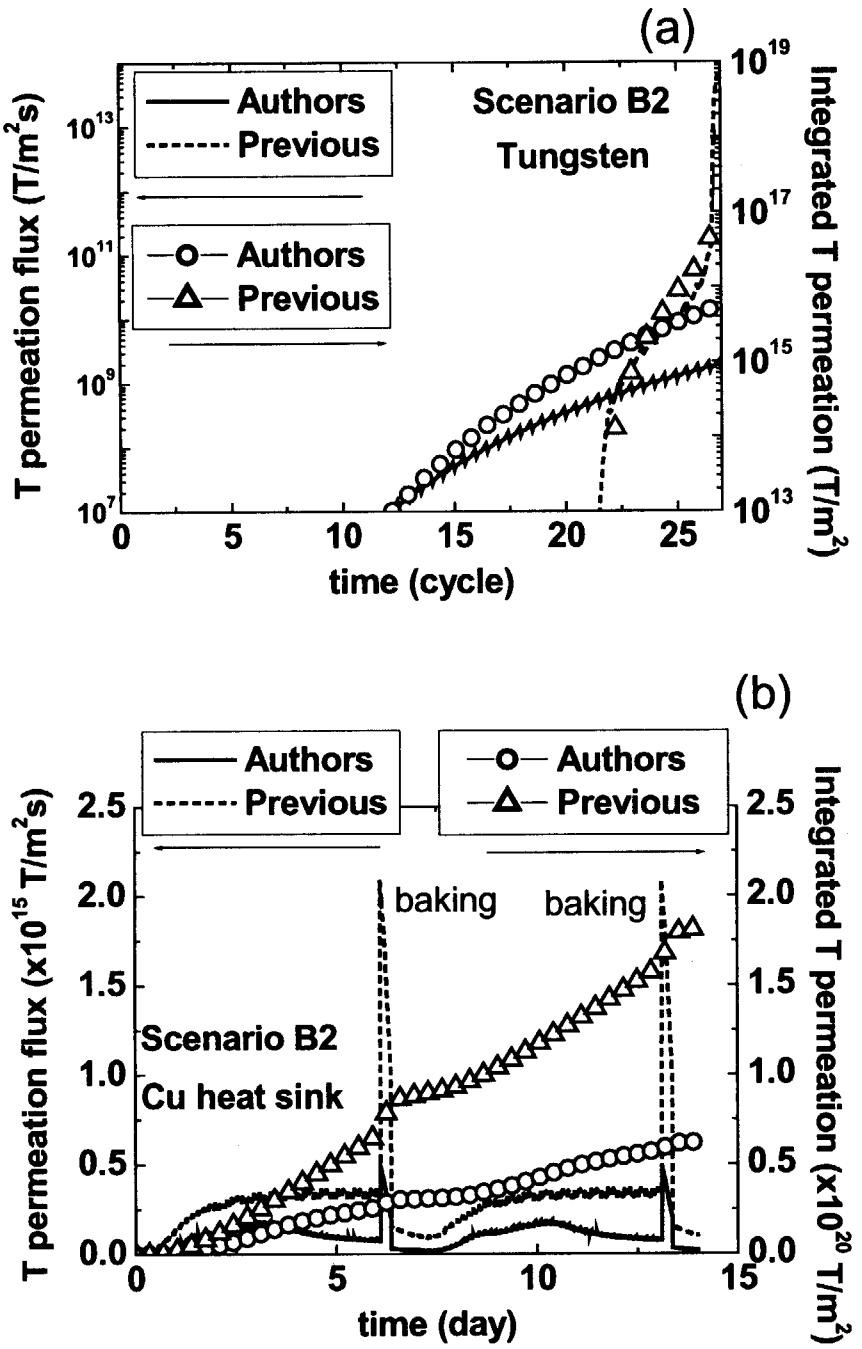

Fig. 5 Time evolution of tritium permeation rate and permeation amount per unit area through (a) tungsten armor region, (b) the copper heat sink region with the authors' data and previous data.

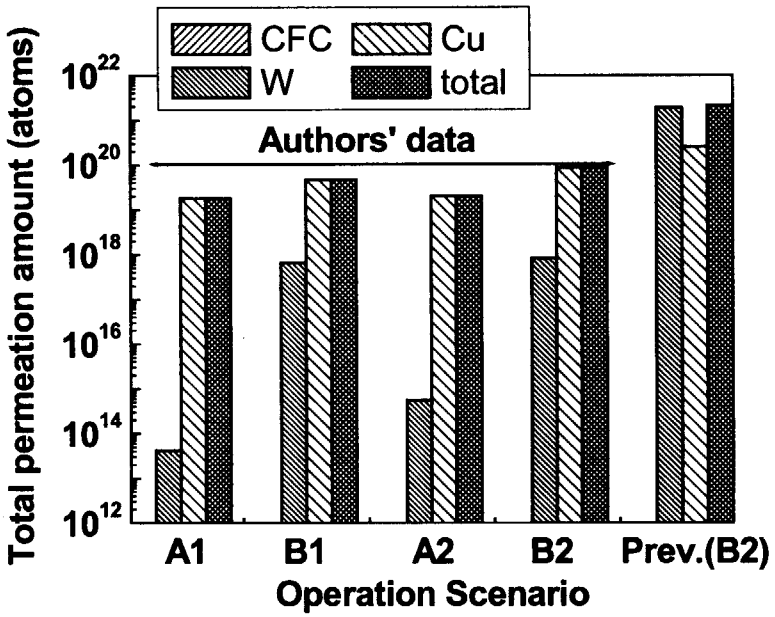

Fig. 6 Tritium permeation amount through the divertor under the various operation scenarios with the authors' data assuming incident flux to the copper region is 0.1% of the armor region. Here, Prev. (B2) is the evaluation result with the previous data under the scenario B2.

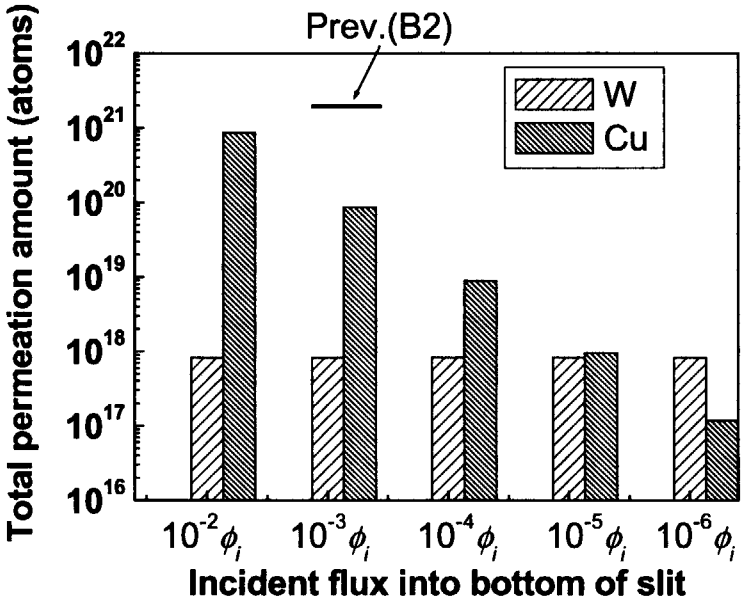

Fig. 7 Dependence of tritium permeation amount on the incident flux into the bottom of the slits (copper region) ranging from 10^{-6} to 0.01 of the incident flux into the armor region (ϕ_i).
Here, Prev. (B2) is the evaluation result with the previous data under the scenario B2.

国際単位系（SI）と換算表

表1　SI基本単位および補助単位

量	名称	記号
長さ	メートル	m
質量	キログラム	kg
時間	秒	s
電流	アンペア	A
熱力学温度	ケルビン	K
物質量	モル	mol
光度	カンデラ	cd
平面角	ラジアン	rad
立体角	ステラジアン	sr

表2　SIと併用される単位

名称	記号
分，時，日	min，h，d
度，分，秒	°，′，″
リットル	l，L
トン	t
電子ボルト	eV
原子質量単位	u

1 eV=1.60218×10^{-19}J

1 u=1.66054×10^{-27}kg

表5　SI接頭語

倍数	接頭語	記号
10^{18}	エクサ	E
10^{15}	ペタ	P
10^{12}	テラ	T
10^{9}	ギガ	G
10^{6}	メガ	M
10^{3}	キロ	k
10^{2}	ヘクト	h
10^{1}	デカ	da
10^{-1}	デシ	d
10^{-2}	センチ	c
10^{-3}	ミリ	m
10^{-6}	マイクロ	μ
10^{-9}	ナノ	n
10^{-12}	ピコ	p
10^{-15}	フェムト	f
10^{-18}	アト	a

表3　固有の名称をもつSI組立単位

量	名称	記号	他のSI単位による表現
周波数	ヘルツ	Hz	s^{-1}
力	ニュートン	N	$m\cdot kg/s^2$
圧力，応力	パスカル	Pa	N/m^2
エネルギー，仕事，熱量	ジュール	J	N·m
工率，放射束	ワット	W	J/s
電気量，電荷	クーロン	C	A·s
電位，電圧，起電力	ボルト	V	W/A
静電容量	ファラド	F	C/V
電気抵抗	オーム	Ω	V/A
コンダクタンス	ジーメンス	S	A/V
磁束	ウェーバ	Wb	V·s
磁束密度	テスラ	T	Wb/m^2
インダクタンス	ヘンリー	H	Wb/A
セルシウス温度	セルシウス度	℃	
光束	ルーメン	lm	cd·sr
照度	ルクス	lx	lm/m^2
放射能	ベクレル	Bq	s^{-1}
吸収線量	グレイ	Gy	J/kg
線量等量	シーベルト	Sv	J/kg

表4　SIと共に暫定的に維持される単位

名称	記号
オングストローム	Å
バーン	b
バール	bar
ガル	Gal
キュリー	Ci
レントゲン	R
ラド	rad
レム	rem

1 Å=0.1nm=10^{-10}m

1 b=100fm^2=10^{-28}m^2

1 bar=0.1MPa=10^5Pa

1 Gal=1cm/s^2=10^{-2}m/s^2

1 Ci=3.7×10^{10}Bq

1 R=2.58×10^{-4}C/kg

1 rad=1cGy=10^{-2}Gy

1 rem=1cSv=10^{-2}Sv

（注）

1．表1－5は「国際単位系」第5版，国際度量衡局1985年刊行による。ただし，1 eVおよび1 uの値はCODATAの1986年推奨値によった。

2．表4には海里，ノット，アール，ヘクタールも含まれているが日常の単位なのでここでは省略した。

3．barは，JISでは流体の圧力を表わす場合に限り表2のカテゴリーに分類されている。

4．EC閣僚理事会指令ではbar，barnおよび「血圧の単位」mmHgを表2のカテゴリーに入れている。

換算表

力	N(=10^5dyn)	kgf	lbf
	1	0.101972	0.224809
	9.80665	1	2.20462
	4.44822	0.453592	1

粘度　1 Pa·s(N·s/m^2)=10 P(ポアズ)(g/(cm·s))

動粘度　1m^2/s=10^4St(ストークス)(cm^2/s)

圧力	MPa(=10bar)	kgf/cm^2	atm	mmHg(Torr)	lbf/in^2(psi)
	1	10.1972	9.86923	7.50062×10^3	145.038
	0.0980665	1	0.967841	735.559	14.2233
	0.101325	1.03323	1	760	14.6959
	1.33322×10^{-4}	1.35951×10^{-3}	1.31579×10^{-3}	1	1.93368×10^{-2}
	6.89476×10^{-3}	7.03070×10^{-2}	6.80460×10^{-2}	51.7149	1

エネルギー・仕事・熱量	J(=10^7 erg)	kgf·m	kW·h	cal(計量法)	Btu	ft·lbf	eV
	1	0.101972	2.77778×10^{-7}	0.238889	9.47813×10^{-4}	0.737562	6.24150×10^{18}
	9.80665	1	2.72407×10^{-6}	2.34270	9.29487×10^{-3}	7.23301	6.12082×10^{19}
	3.6×10^6	3.67098×10^5	1	8.59999×10^5	3412.13	2.65522×10^6	2.24694×10^{25}
	4.18605	0.426858	1.16279×10^{-6}	1	3.96759×10^{-3}	3.08747	2.61272×10^{19}
	1055.06	107.586	2.93072×10^{-4}	252.042	1	778.172	6.58515×10^{21}
	1.35582	0.138255	3.76616×10^{-7}	0.323890	1.28506×10^{-3}	1	8.46233×10^{18}
	1.60218×10^{-19}	1.63377×10^{-20}	4.45050×10^{-26}	3.82743×10^{-20}	1.51857×10^{-22}	1.18171×10^{-19}	1

1 cal= 4.18605J（計量法）

= 4.184J（熱化学）

= 4.1855J（15℃）

= 4.1868J（国際蒸気表）

仕事率　1 PS(仏馬力)

= 75 kgf·m/s

= 735.499W

放射能	Bq	Ci
	1	2.70270×10^{-11}
	3.7×10^{10}	1

吸収線量	Gy	rad
	1	100
	0.01	1

照射線量	C/kg	R
	1	3876
	2.58×10^{-4}	1

線量当量	Sv	rem
	1	100
	0.01	1

（86年12月26日現在）

Tritium Permeation Evaluation through Vertical Target of Divertor based on Recent Tritium Transport Properties